HiSST: 3rd International Conference on
High-Speed Vehicle Science Technology
14 -19 April 2024, Busan, Korea

Heterodyne Dual Frequency Comb Laser Absorption Spectroscopy Measurements in Supersonic Combustion

Jan Martinez Schramm[1], Leni Schmidt[2]

Abstract

Experimental determination of NO and H_2O production during hydrogen combustion applying laser absorption spectroscopy has been performed in the High Enthalpy Shock Tunnel Göttingen of the German Aerospace Center. The combustion process forming these species within the propulsion unit of a small scale wind tunnel model was experimentally studied. A novel experimental approach to obtain absorption spectra in the infrared region within µ-seconds is reported. This technique is based on the use of quantum cascade lasers generated frequency combs and enables multi-species measurements at high acquisition rates. The generated frequency combs are within the 1740±20 cm^{-1} wavenumber region which features strong NO and H_2O spectral lines allowing for the spectral characterization of these species. The technique and its underlying physics, the application in short duration ground testing and the needed calibration work is discussed.

Keywords: hypersonic flow, shock tunnel experiments, laser absorption, hydrogen combustion, dual comb frequency quantum cascade laser, High Enthalpy Shock Tunnel Göttingen, HEG, EU Stratofly

Nomenclature

h	– specific enthalpy
l	– absorption path length
Ma	– Mach number
m_{O2}	– mass flow rate of oxygen
n	– mole fraction/ concentration
ρ	– flow density
p	– pressure
p_0	– reservoir pressure
p_{t2}	– Pitot pressure
q_{t2}	– stagnation point heat flux
Re	– Reynolds number
T	– temperature
Δt_{stab}	– stabilisation time
u	– free-stream velocity
U	– voltage
RF	– radio frequency
QCL	– quantum cascade laser

1. Introduction

Sustainability is one of the main driving factors in current research on civil aviation. While the environmental dimension requires new aviation concepts to consider CO_2 emissions, there is also the desire for performance improvement by reducing the transfer time of long-range flights from an economic point of view. In this context, various concepts for high-speed vehicles are developed. The use of hydrogen combustion-based scramjets as propulsion units to drive hypersonic passenger transport is part of the ongoing investigations. Although hydrogen-fuelled vehicles prevent CO_2 emission, the formation of NO and H_2O as emission gases during the combustion process may have other environmental effects. Therefore, the experimental determination of NO and H_2O production in hydrogen combustion is of interest and is part of the study in the High Enthalpy Shock Tunnel Göttingen (HEG), one of the major European hypersonic test facilities. The test time for experiments in HEG lies typically

[1] *German Aerospace Center (DLR), Bunsenstraße 10, 37073 Göttingen, Germany, Jan.Martinez@dlr.de*
[2] *Von-Karman-Institute, Waterloosesteenweg 72, B-1640 Sint-Genesius-Rode, Belgium, Leni.Schmidt@vki.ac.be*

in the ms range, which requires measurements techniques with high acquisition rates and high precision. The applicability of the heterodyne dual frequency comb-based absorption spectroscopy with quantum cascade lasers (QCLs) in the infrared region within µ-second range has been demonstrated at the High Enthalpy Shock Tunnel Göttingen, HEG, of the German Aerospace Center, DLR [1]. Since the first application at HEG, the technique has been developed further and new measurement modes are implemented. These modes enable higher resolution measurements by modulating the laser current and temperature to change the spectral point spacing of the spectrometer. One of the main goals of the calibration study discussed, is to identify whether the use of optical fibers in the experimental setup lead to influences in signal and how the measurement results are affected by that. Calibration measurements are performed in a laboratory set-up to evaluate the accuracy and quality of the different measurement modes. The paper describes the experimental prerequisites for the measurements, and demonstrates the resulting comparison for the measurement modes.

2. Quasi Heterodyne Dual Comb Laser Absorption Spectroscopy

Good spectral resolution and wide coverage or high signal-to-noise ratio with short measurement times are rarely easily combined for different spectroscopic techniques: single wavelength spectrometers only allow one narrow band measurement with high resolution, while Fourier transform spectroscopy (FTIR) measures broadband with rather low resolution. Often FTIR systems includes the handling of moving parts [3]. High-resolution molecular spectroscopy is important for many different fields of applications, including combustion diagnostics where the challenge is to observe multiple species on short time scales. Especially the mid-IR spectral domain is of interest since fundamental vibrational excitations are located in this range. The High-resolution molecular spectroscopy was revolutionized by the advent of frequency combs whose generation is enabled by high-power quantum cascade lasers (QCLs). Frequency combs were first introduced to improve the precision of frequency measurements [4]. A single frequency comb is characterized by a finite number of sharp spectral lines that are distanced by a repetition frequency f_{rep} at a given offset frequency f_{ceo} [5]:

$$f_n = n \cdot f_{\mathrm{rep}} + f_{\mathrm{ceo}}.$$

Importantly, the line-spacing (or f_{rep}) of frequency combs is extremely well defined, making them useful for spectroscopy. If two frequency combs with slightly different repetition frequencies $f_{\mathrm{rep},1}$ and $f_{\mathrm{rep},2}$ are combined, a heterodyne beating with a difference frequency of $\Delta f_{\mathrm{rep}} = f_{\mathrm{rep},2} - f_{\mathrm{rep},1}$ is created [6]. Since this set-up directly links the frequency comb from an optical domain to the radio frequencies, RF, it is possible to take measurements using conventional frequency counters [5]. The difference frequencies lie in our case in the RF range that falls within the detector's limits (< 10 GHz).

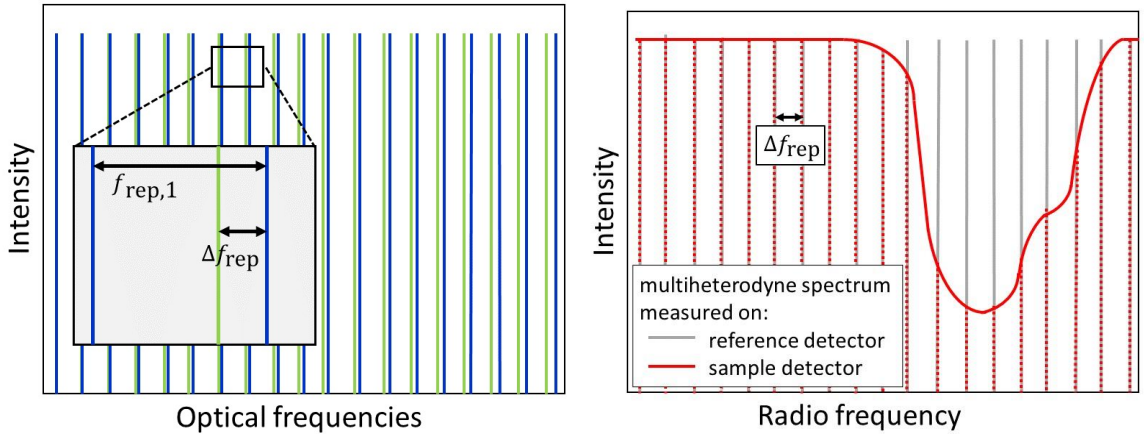

Fig. 1 The left figure illustrates two frequency combs with slightly different repetition frequencies, generated by the QCLs. The figure on the right gives an exemplary resulting heterodyne beating, where the sample beam is affected by an absorption feature, while the reference beam reaches the detector without attenuation.

This use of two frequency combs with the multi-heterodyne detection, so-called dual-comb spectroscopy, enables Fourier transform spectroscopy with high resolution, high sensitivity, and no moving parts. By tuning a frequency comb via current or temperature, the comb's repetition frequency

is changed, resulting in heterodyne with slightly changed difference frequency which allows measurements at diverse spectral points. As this sweeping procedure reduces the spectral point spacing, a spectrum has a higher resolution. In the HEG, combustion experiments are conducted; during hydrogen combustion, NO and H_2O are the main species that are investigated. Fig. 2 (left) presents a broad NO and H_2O absorption spectra for a typical hydrogen combustion flow case (p = 4.2 bar, T = 2300 K) in a scramjet small-scale experiment in HEG [1]. Fig. 2 (right) shows features of the absorption spectra in the emission region of the QCLs used. The absorption lines of both species to be inspected (H_2O and NO) can be separated and the reconstruction of the state of both species can be performed within one measurement.

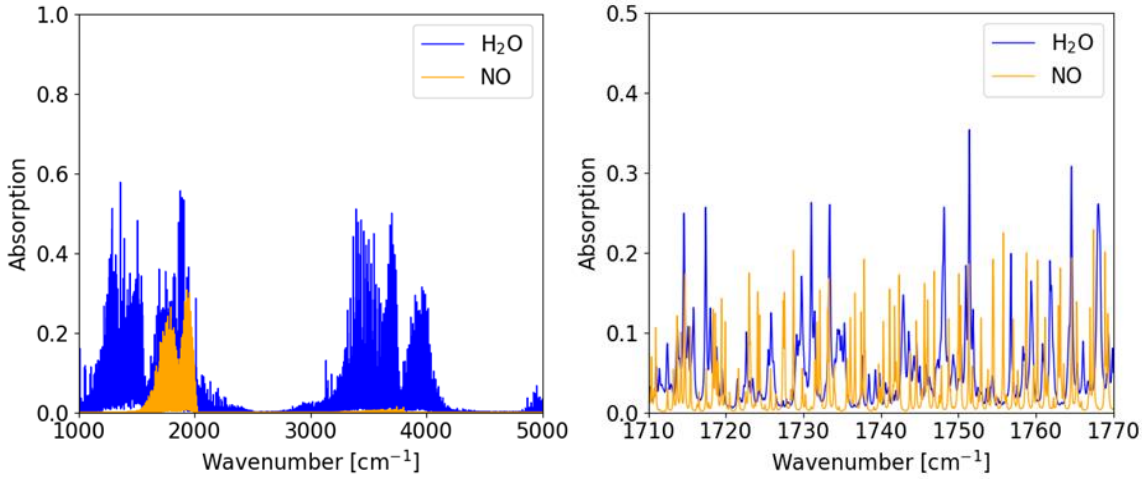

Fig. 2 Broad (left) and narrow (right) absorption spectra of NO and H_2O for a hydrogen combustion flow case in HEG (p = 4200 mbar, T = 2300 K, l = 6.6 cm, η_{H2O} = 0.08, η_{NO} = 0.03) simulated with HITRAN database [8].

3. Spectrometer

The commercially available dual-frequency-comb spectrometer IRis-F1 (IRsweep AG, Switzerland) uses two closely matched QCL frequency comb sources emitting at a center frequency of 1740 cm^{-1} with a span of 40 cm^{-1} and a standard repetition rate of 0.25 cm^{-1}. A schematic of the spectrometer is shown in Fig. 3. The spectrometer is operated in amplitude sensitive configuration, which means the beams from both QCLs are combined through a beam splitter in the laser module and pass together through the sample before being detected on a thermoelectrically cooled detector. The reference beam reaches the detector without disturbances.

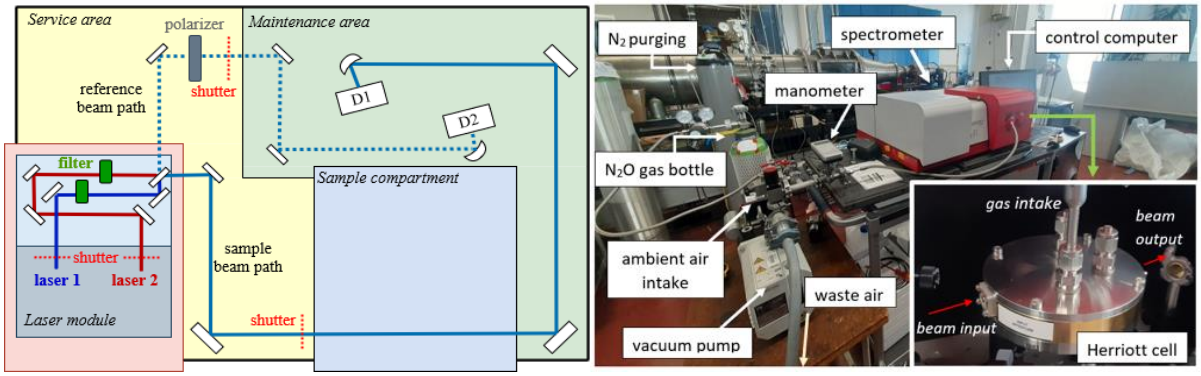

Fig. 3 Left: Beam path inside the spectrometer. The QCLs generate two frequency combs that are combined with a beam splitter. Sample (solid) and reference (dotted) are aligned on detectors D1 and D2, respectively. Right: Experimental set-up with internal Herriott cell.

The spectrometer allows for different measurement modes shown in

Fig. **4**. The modes *LongTerm* and *TimeResolved* use a fixed spatial resolution, while the measurement time can be varied. In *LongTerm* mode, a single spectrum is obtained from averaging multiple number of measurements; in *TimeResolved* mode, multiple measurements are taken, yielding a spectrum for each time instant. Both these modes leave the lasers current and temperature constant throughout the acquisition allowing time resolutions at *4 µs* and a spectral point spacing of *0.25 cm^{-1}* [5]. The tuning of the QCLs frequency comb emission frequencies via temperature and current reduces the gaps between adjacent lines to be observed. By alternately and stepwise increasing the current of both lasers in *StepSweeping* mode, the gaps between points are closed without moving the multiheterodyne beat note to frequencies outside the detection bandwidth [7]. To prevent possible QCL mode switches during operation or the generation of subcombs due to a too large current tuning range, it is necessary to define a suitable current ramp consisting of stepwise tuning of the currents. By sweeping through this ramp at different temperatures, the gap is filled. After every current or temperature step, the lasers wait for a given stabilization time Δt_{stab} before continuing the acquisition. The standard stabilization times for current and temperature steps are Δt_{stab} = 0.7 s and 60 s, respectively. This method decreases the spectral point spacing to 10^{-3} cm^{-1} (

Fig. **4**). In *FastSweeping* mode, only the current of the lasers is periodically modulated in a saw-tooth wave at a rate of 5 mA/V, by a wave generator. The temperature is constant and the current modulation does not include stabilization times. Each ramp is set to increase from U = 0 V to approximately U = 6 V and takes about 1 ms to sweep through. The ramps are recorded and thus, the frequency changes can be precisely coordinated in the post-processing. This method decreases the time resolution of the measurements, but increases the spectral resolution by a factor of almost 250 (theoretical value when sampling with 4 µs during 1 ms).

During operation, the spectrometer is continuously purged with N_2. Before starting a measurement, transfer functions are taken with the lasers light blocked. These functions eliminate the electronic background signals of the system itself. To investigate the accuracy of the different measurement modes, experiments with exactly known conditions are carried out and compared with the reference spectra simulated with the HITRAN database [8].

4. Calibration

By reflecting a beam multiple times in a circular shaped cell with a series of curved Au coated mirror segments on the wall, a Herriott cell achieves a long path length (here: 4 m) within a compact volume und hence is practical for precise absorption measurements. The cell is placed inside the spectrometer's sample compartment and filled with either N_2O or ambient air containing water (8500 ppm). The water content was determined by measuring temperature and relative humidity of the surrounding air.

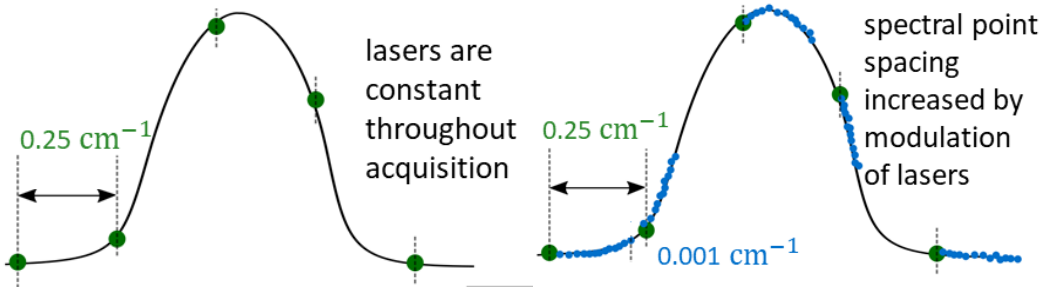

Fig. 4 Overview of the two basic measurement modes used for the laser absorption technique. On the left-hand side constant spatial resolution (*LongTerm*, *TimeResolved*) and on the right-hand side tuned operation with varying spatial resolution (*StepSweeping*, *FastSweeping*).

The species NO was not selected as a calibration test gas since it is only weakly absorbing at room temperature and is thus not optimal for the purpose of this calibration work. Prior to the sample measurements, the cell is in vacuum and a background measurement is taken. The comparison between spectra before and after gas inlet allows observing the gas content. Measurements are taken varying the measurement modes and pressures p (100, 300, 500, 700 and 900 mbar). As the *FastSweeping* mode modulated the laser current on a millisecond scale without any laser stabilization time, while for *StepSweeping* we let the lasers stabilize, the current stabilization time is varied in the *StepSweeping* measurements between Δt_{stab} = 0.7 and Δt_{stab} = 0.00001 s to understand this influence. Results

obtained in *LongTerm* mode are given in Fig. 5 for H_2O and N_2O at p = 500 mbar. The data at the measured spectral positions align well with the simulated HITRAN reference spectrum. But it has to be noted that not all absorption features are fully resolved. As inferred from a detailed closer view on specific features (Fig. 5, right plot), it is obvious that the spectral distance is too large between adjacent spectral points. This issue may, if needed be overcome by using the *StepSweeping* mode.

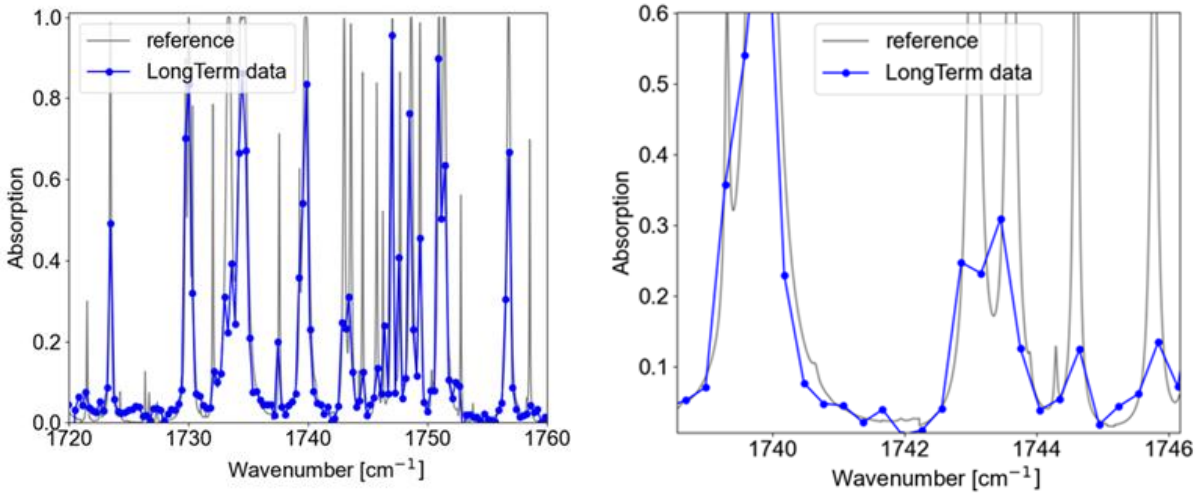

Fig. 5 Absorption spectra obtained for ambient H_2O (left) and zoom of the data to the right. The data were obtained used the *LongTerm* measurement mode of the spectrometer.

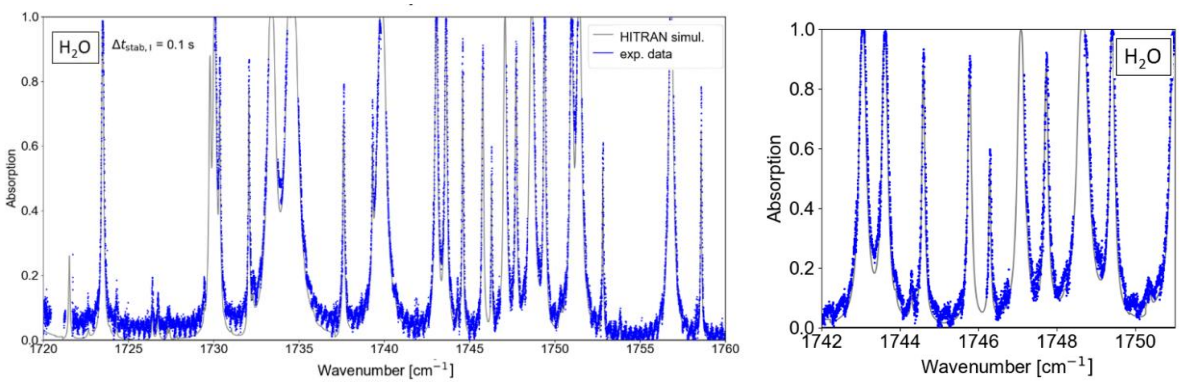

Fig. 6 Absorption spectra obtained in *StepSweeping* mode for H_2O at p = 500 mbar shown on the left with a detailed view on the right. The data confirms that the *StepSweeping* mode reduces the large spectral point distance successfully and thus all absorption features are resolved better as compared to the spectral data obtain in Fig. 5.

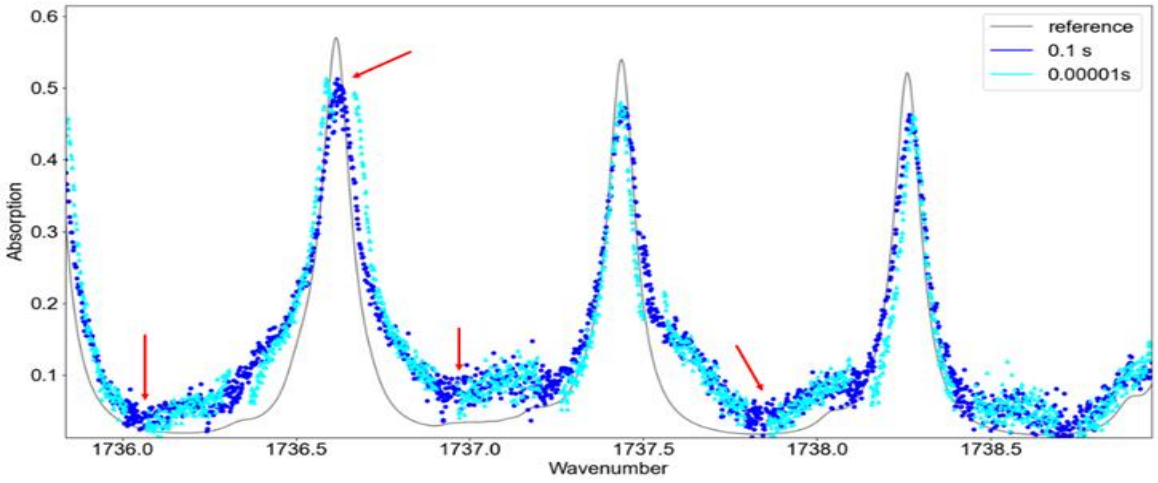

Fig. 7 Measurements with different current stabilization times align. Red arrows indicate that gaps are not completely filled for shorter stabilization time.

For a stabilization time of the current applied of Δt_{stab} = 0.1 s, the obtained spectra for p = 500 mbar are given Fig. 6. The left side graph shows the spectra obtained for complete measurement range, the right side graph shows a more detailed part of it. If Fig. 5 and Fig. 6 are compared directly, the increased spectral resolution results in a complete detection of all absorption features. As the current stabilization time was varied for different measurements, the absorption spectra are compared with regard to possible changes in the accuracy or shape of peaks. The comparison for two different stabilization times of the current, namely $\Delta t_{\mathrm{stabI}}$ = 0.1 s and Δt_{stab} = 0.00001 s, is given in Fig. 7. On first view, the spectra are quite similar by eye; nevertheless, it has to be noted that a shorter stabilization time results in gaps in the absorption spectrum as exemplary highlighted with the red arrows in Fig. 7. This can be explained by the fact that the lasers do not have much time to stabilize completely, they don't completely adapt to the pre-defined currents and thus the defined current range is not fully exploited as for measurements with longer stabilization time. A qualitative comparison of all the measured data for the different pressures and stabilization times is done based on the RMS. The RMS was calculated for deviations of experimentally measured amplitudes to the reference HITRAN amplitudes for all spectral measurement points. This results in an average of two measurement series with same conditions in each case and the data is presented in Fig. 8. For a decreasing stabilization time, the RMS tends to slightly rise. Over the entire stabilization time range, the observed maximum increase is plus 3% (for H_2O at p = 100 mbar), while the RMS on average over all measurements increases by around 1% between Δt_{stab} = 0.7 s and $\Delta t_{\mathrm{stab,\,I}}$ = 0.00001 s, so it does not change significantly. Considering that the current stabilization time is reduced over almost five orders of magnitude, the deviation is negligible. The current stabilization time is, in first order, equal to the acquisition rate which can be achieved.

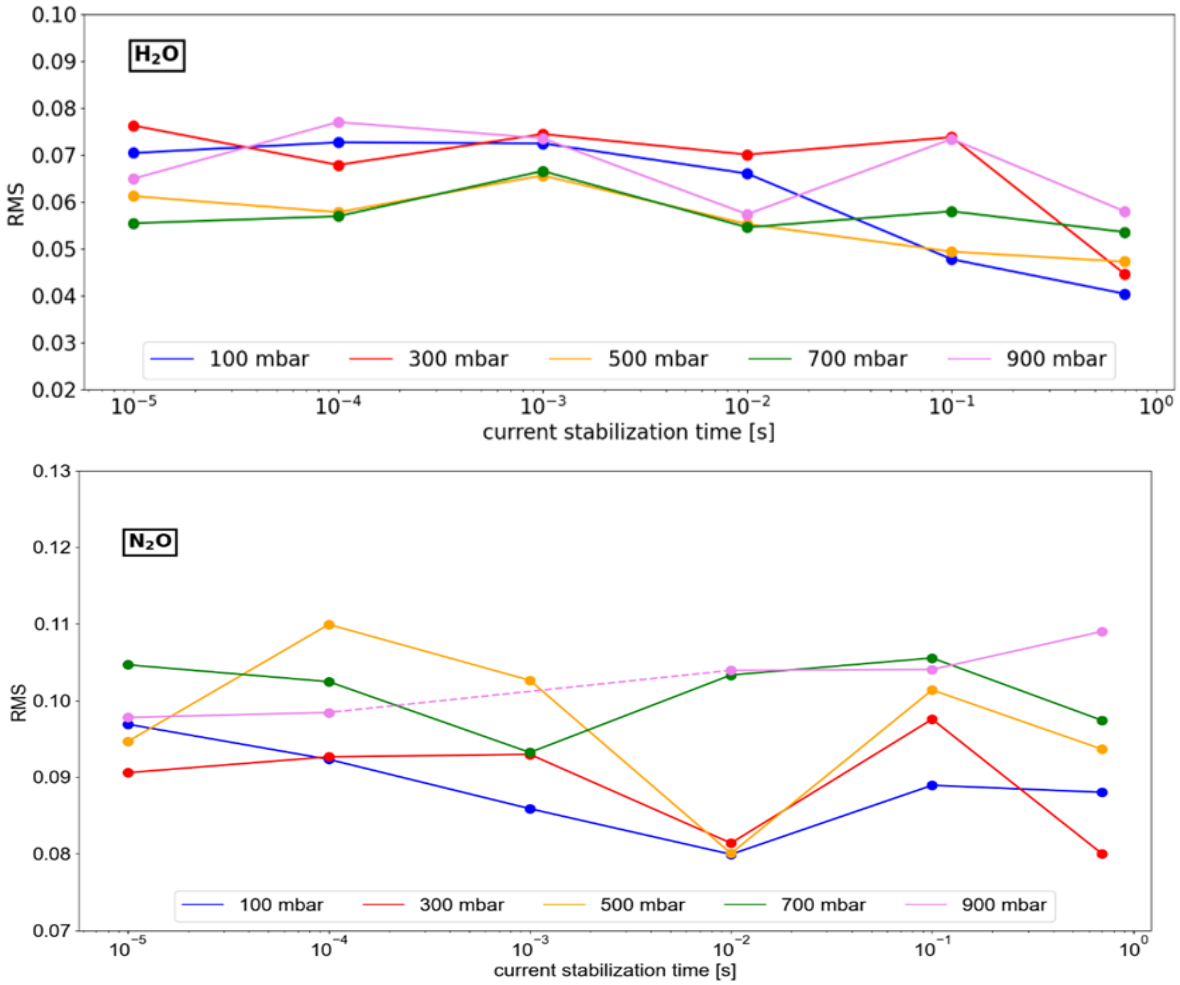

Fig. 8 The calculated RMS for H_2O (top) and N_2O (bottom) for different stabilization times and pressures, averaged over two measurements. The measurements are obtained with the internal Herriot cell. Please

note that the stabilisation time $\Delta t_{\mathrm{stab,\,I}}$ of the current applied to the laser heads spans five orders of magnitude.

An experimental calibration of the measurement modes of dual-comb spectrometer was performed. The *StepSweeping* mode allows high spectral resolution and hence enables high precision spectroscopic measurement in good consistency with theoretical data. A variation of the stabilization time showed a negligible effect on the accuracy of the measurement, thus promising good results for the use of *FastSweeping* mode.

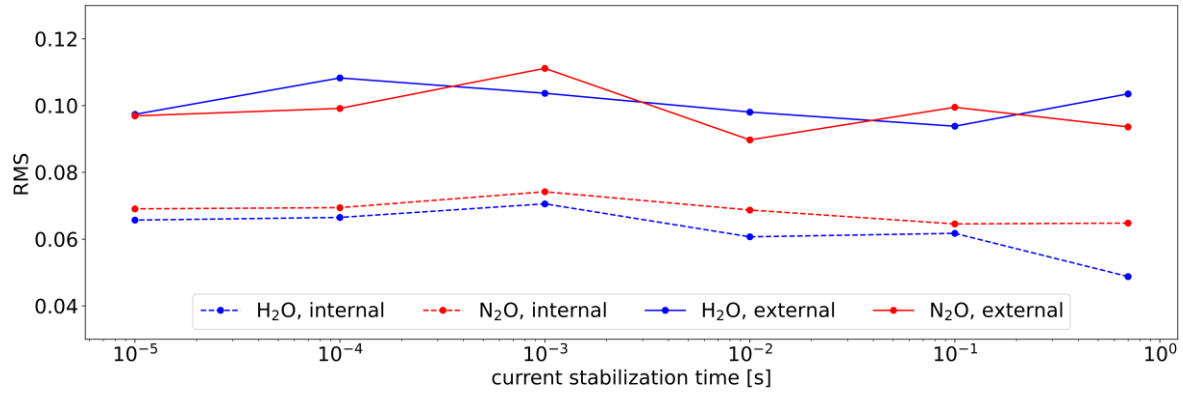

Fig. 9 The calculated RMS for H_2O and N_2O in dependence of different stabilization times. The results for the varying pressures are all averaged. The measurements are obtained with the Herriot cell placed internally into the spectrometer and externally with the laser light couples by fibres into the Herriot cell.

The calibration work is continued with the Herriott cell being placed externally to investigate the influence of optical fibers that guide the sample-beam out and back to the spectrometer. This setup demands additional optics for the in- and out-coupling of the beam. It is relevant to understand how the signal is affected by this procedure. Challenges here are both the general power loss due to the fibers as well as occurring back reflections from the fiber facets, which caused negative optical feedback (fringing). However, with the external Herriott cell, measurements with the same previous parameters are repeated and the RMS is only slightly increased compared to the results obtained with internal Herriott cell (Fig. 9). We can summarize at this point, that the influence of the fibres is visible in the calibration data, but is of small influence on the overall error. The trend that the error is smaller for long stabilization times of the QCK heads is identical for internal or external measurements.

5. Combustion Experiments

Experiments have been conducted in the High Enthalpy Shock Tunnel (HEG) of the German Aerospace Center, DLR. The HEG is designed on the working principle of a free piston driven shock tube (Stalker tube [9]) and is one of the major European hypersonic test facilities of this kind. Additional information about the working principle of the facility, its capabilities and former use in combustion research can be found in Ref. [10–15]. The operating condition that has been used for the experimental campaign is the nominal condition H3.3R3.7 (former condition XIII). Table 1 lists the nominal reservoir conditions for the nozzle, the Pitot pressure p_{t2} and stagnation point heat flux q_{t2}, as well the complete set of free stream parameters. The subscript *0* refers to the reservoir conditions and *t2* to the total conditions behind the normal shock. The other variables p yield pressure, T temperature, h specific enthalpy, u velocity, Ma Mach number, Re Reynolds number, ρ density, and m_{O2} mass flow rate of oxygen. The total available test time is approximately 5 ms. Based on the nozzle reservoir conditions, the free stream is determined by numerical computation of the nozzle flow [11, 13–15].

p_0 [MPa]	T_0 [K]	h_0 [MJ/kg]	170
	2740	3.3	

p_{t2} [kPa]	q_{t2} [MW/m²]
146.53	3.71

p [Pa]	T [K]	ρ [g/m^3]	u [m/s]	m_{O_2} [g/m^3]	Ma [-]	Re [1/m]
1990	266	25.9	2398	6.34	7.4	$3.7 \cdot 10^{-6}$

Table 1 Operating condition of the High Enthalpy Shock Tunnel for the experiments reported.

The supersonic hydrogen combustion flow to be studied is generated in the propulsion unit of the SFFE wind tunnel model. SSFE stands for small scale flight experiment. This configuration is based on the full scale LAPCAT (Long- Term Advanced Propulsion Concepts and Technologies) II Mach 8 MR 2 vehicle proposed by ESA-ESTEC as described in Ref. [16]. The MR 2 vehicle is characterized by the combination of an aerodynamic efficient wave rider configuration and the dorsal integration of a high performance propulsion unit whose cruise and aero-propulsive performance was numerically assessed [17]. The SSFE configuration was derived from the MR2 as reported in Ref. [18, 19]. Further details about the model design are given in Ref. [20,21]. The combustor layout is shown in Fig. 10. Two semi struts and one full strut injector expand the hydrogen into the combustor. The generation of NO in the combustion process is visualized by iso surfaces from the numerical rebuilding of the combustor flow. Additionally, the lines of sight for the laser absorption spectroscopy measurements are shown. Numerical simulation on the test case has been performed and published [22]. The data set have been used to reconstruct the absorption spectra for H_20 and NO along the lines of sight given in Fig. 10.

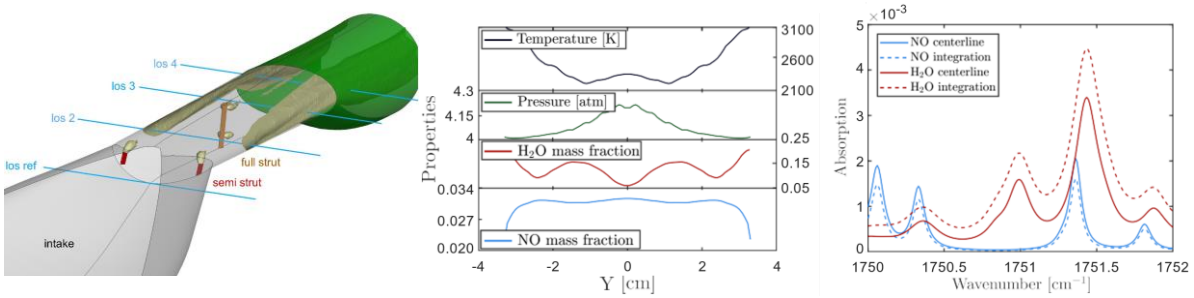

Fig. 10 Left: Schematic view of the combustor section of the SSFE. Shown are the lines of sight (LOS) of the IR laser path of the absorption spectroscopy system through the combustor, additionally the semi- and full strut injectors are shown with iso surfaces of mass fractions of NO. Right: Schematic of the SSFE model with the optical couplers installed on the outer part of the model and a photograph showing of an optical coupler installed on the model.

The graph in the middle of Fig. 10 shows the temperature and pressure distribution along a line of sight through the combustor obtained from the numerical data [22]. The mass fractions of both species are also given. The resulting absorption spectra from the calculations are given in the right-hand side plot in Fig. 10. Two types of post-processing are compared, in the first case, the gas state at the center of the combustor has been used together with the integration length of the line of sight to calculate the corresponding spectra (solid lines in the right-hand side graph in Fig. 10).

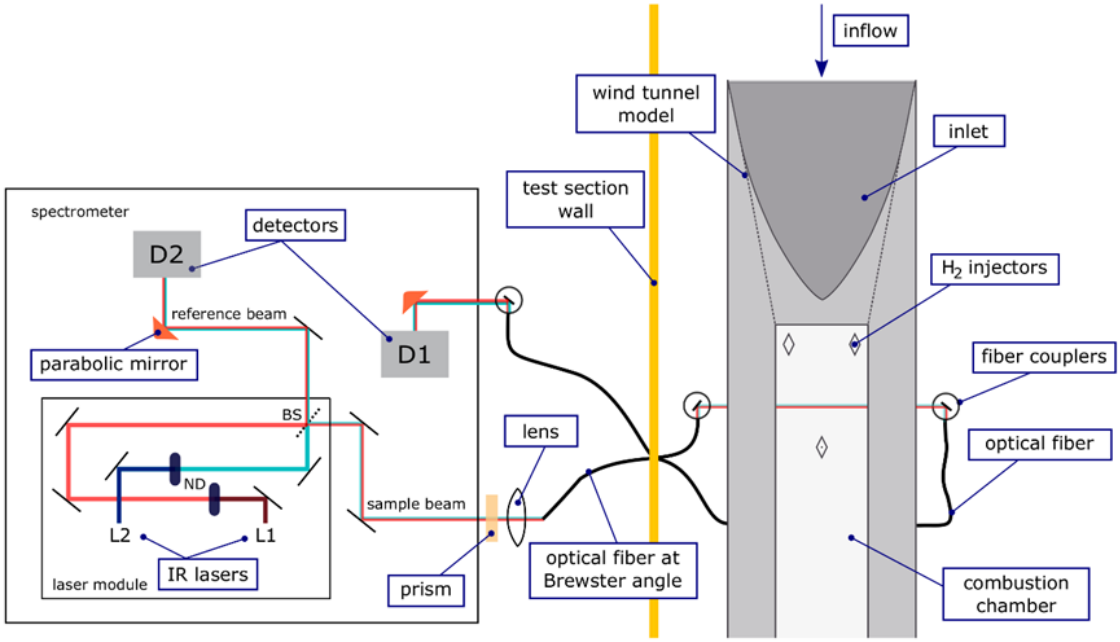

Fig. 11 Schematic of the IR laser beam path inside the spectrometer, the coupling to into the fibers and the outcoupling into the model's combustion chamber.

The second case, given as the dotted lines in the right-hand side graph in Fig. 10, calculates the spectra by integrating through the line of sight considering the changes in pressure, temperature and mass fractions along the line of sight. It can be seen, that the latter method is the favorable one. The comparison to the numerically obtained spectra was performed with the second approach. During the test of SSFE in HEG, the spectrometer has been placed as close as possible to the wind tunnel test section, in order to use a setup having a minimal length of the optical fibers. The fibers are feed through the wind tunnel wall and are attached to fiber couplers installed on the model. The setup is shown schematically in Fig. 11.The final results obtained are summarized in Fig. 12. Here, the experimental obtained mass fractions along the various lines of sight at different streamwise positions x in the combustion chamber of the SSFE model are given. The left-hand side plot combines the experimental and numerical results for the species NO and the right-hand side plot shows the results of H_2O. The figures compare the measurements without any combustion (fuel-off) and with combustion (fuel-on).

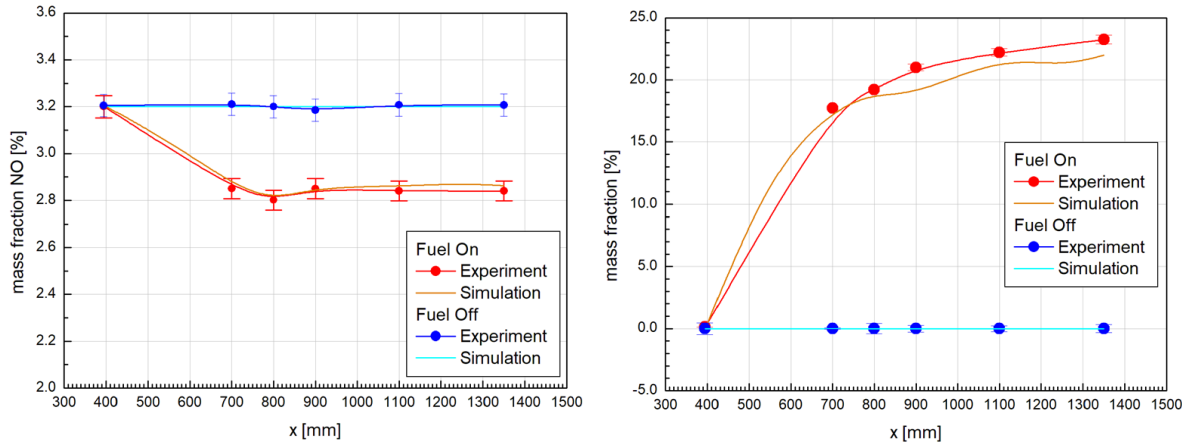

Fig. 12 Results of the mass fraction measurements integrated along the lines of sight of IR laser beam. The left graph shows the distribution of the mass fraction of NO and the right-hand side graph shows the distribution of H_20. Additionally, to the experimental data numerical results are shown.

It has to be noted, that the NO concentration exhibits already a mass fraction level of 3.2% before any combustion takes place. This is due to the fact, that the wind tunnel itself generates NO in the nozzle reservoir which arrives in the free stream (see Table 1) and is compressed into the intake and the

combustion chamber. This amount of free NO has also been modelled numerically. The combustion process reduces the amount of NO to an average mass fraction of about 2.7%. In summary we see a fair agreement between the numerical solutions and the experimental obtained species concentrations.

6. Conclusion

The work conducted at the German Aerospace Center to setup a laser absorption spectroscopy measurement technique has been reported and an extended calibration of the system has been described. The calibration focused on the influence of fibers used to guide the laser light into the wind tunnel model during the experiences. An experimental campaign in the High Enthalpy Shock Tunnel Göttingen has been performed in order to measure NO and H_2O production during hydrogen combustion and the final results have been reported. This novel experimental approach to obtain absorption spectra of both species in the infrared region within µ-second range resulted in good experimental results. The technique is based on the use of frequency combs generated with quantum cascade lasers. It has been demonstrated that this technique enables multi-species measurements at rapid acquisition rates. The pre-analysis of numerical simulations of the supersonic hydrogen combustion flow with respect to the absorption spectral distribution lead to the selection of frequency combs within the 1740 ± 20 cm^{-1} wavenumber region which contains strong NO and H_2O spectral lines. A numerical method to obtain integrated line of sight spectral absorption spectra was created and it was demonstrated that it is necessary to include the boundary layer gas state in the simulation to allow a more exact comparison. A calibration method was reported and its importance was shown with the help of parametric studies of the absorption line spectra in a reference Herriot cell.

7. Acknowledgments

The experimental campaign and the associated research work on the experimental findings has been conducted within the framework of the H2020 STRATOFLY Project, which has received funding from the European Union's Horizon 2020 Research and Innovation Programme under Grant Agreement No. 769246.

References

1. Martinez Schramm, J., Luís, D.: Experimental Approach on Concentration Measurements of NO in Hydrogen Combustion Based on Heterodyne Laser Absorption Spectroscopy Using Quantum Cascade Lasers. In: Dillmann, A., et al. (eds.): STAB/DGLR Symposium 2020, NNFM 151, pp. 110–120. Springer (2021)
2. Schmidt, L., Martinez Schramm, J.: Calibration of Heterodyne Dual Frequency Comb Laser Absorption Spectroscopy for NO and H2O Detection. In: New Results in Numerical and Experimental Fluid Mechanics XIV - Contributions to the 23rd STAB/DGLR Symposium Berlin, Germany 2022. Springer (2022)
3. Griffiths, P.R., De Haseth, J.A., Winefordner, JD.: Fourier Transform Infrared Spectrometry. Wiley (2007)
4. Udem, T., Holzwarth, R., Hänsch, T.W.: Optical frequency metrology. Nature, vol. 416, no. 6877, Art. no. 6877, (2002)
5. Faist, J., Villares, G., Scalari, G., Rösch, M., Bonzon, C., Hugi, A., Beck, M.: Quantum cascade laser frequency combs. Nanophotonics 5(2), 272–291 (2016)
6. Villares, G., Hugi, A., Blaser, S., Faist, J.: Dual-comb spectroscopy based on quantum-cascade-laser frequency combs. Nat Commun, vol. 5 (2014)
7. Lepère, M., Browet, O., Clément, J., Vispoel, B., Allmendinger, P., Hayden, J., Eigenmann, F., Hugi, A., Mangold, M.: A mid-infrared dual-comb spectrometer in step-sweep mode for high-resolution molecular spectroscopy. Journal of Quantitative Spectroscopy & Radiative Transfer (2022)

8. Gordon, I.E. et al.: The HITRAN2020 molecular spectroscopic database. Journal of Quantitative Spectroscopy and Radiative Transfer. Vol. 277, p. 107949. (2022)
9. Stalker, R.J.: A study of the free-piston shock tunnel. AIAA Journal, 5(12), (1967). https://doi.org/10.2514/3.4402.
10. Hannemann, K. et al.: The High Enthalpy Shock Tunnel Göttingen of the German Aerospace Center (DLR). Journal of large-scale research facilities, 4(A133), (2018). http://dx.doi.org/10.17815/jlsrf-4-168.
11. Hannemann, K., Martinez Schramm, J.: High Enthalpy, High Pressure Short Duration Testing of Hypersonic Flows. Springer Handbook of Experimental Fluid Mechanics. Springer-Verlag Berlin Heidelberg (2007)
12. Hannemann, K., Martinez Schramm, J., Karl, S.: Recent extensions to the High Enthalpy Shock Tunnel Göttingen (HEG). In: Proceedings of the 2nd International ARA Days "Ten Years after ARD", Arcachon, France, 21-23 October (2008)
13. Hannemann, K.: High Enthalpy Flows in the HEG Shock Tunnel: Experiment and Numerical Rebuilding. In 41st AIAA Aerospace Sciences Meeting and Exhibit, Reno, NV, 6-9 June (2003). https://doi.org/10.2514/6.2003-978
14. Hannemann, K. et al.: The influence and delay of driver gas contamination in HEG. In 21st AIAA Aerodynamic Measurement Technology and Ground Testing Conference, AIAA 2000-2593, Denver, CO, (2000). https://doi.org/10.2514/6.2000-2593
15. Hannemann, K., Krek, R., Eitelberg, G.: Latest Calibration Results of the HEG Contoured Nozzle. In B. Sturtevant, J.E. Sheperd, and H.G. Hornung, editors, Proceedings of the 20th International Symposium on Shock Waves, pages 1575– 1580, Pasadena, CA, July 1995. World Scientific, (1996)
16. Steelant, J., Langener, T.: The LAPCAT-MR2 Hypersonic Cruiser Concept. In ICAS-2014-0428, 29th Congress of the International Council of the Aeronautical Sciences, St. Petersburg (2014)
17. Roncioni, P. et al.: Numerical Simulations and Performance Assessment of a Scram- jet Powered Cruise Vehicle at Mach 8. Journal of Aerospace Science and Technology, 42:218–228, (2015). https://doi.org/10.1016/j.ast.2015.01.006
18. Langener, T., et al.: Layout and Design Verification of a Small Scale Scramjet Combustion Chamber. In Proceedings 21st International Symposium on Airbreathing Engines (2013).
19. Langener, T. et al.: Design and Optimization of a Small Scale M= 8 Scramjet Propulsion System. In Space Propulsion 2012, Bordeaux: AAAF/ESA/CNES (2012)
20. Martinez Schramm, J. et al.: Design and manufacturing of a modular small scale M8 scramjet flight experiment configuration wind tunnel model, LAPCAT-II, d.5.2.4 edition, (2013)
21. Martinez Schramm, J. et al. Ground testing synthesis of the lapcat ii small scale flight experiment configuration scramjet flow path. In 20th AIAA International Space Planes and Hypersonic Systems and Technologies Conferences, Glasgow, Scotland (2015). https://doi.org/10.2514/6.2015-3627.
22. Saccone, G. et al.: Kinetic Analysis and CFD Modelling of Hydrogen-Air Combustion Applied to Scramjet Vehicles, Proceedings of the 7th World Congress on Momentum, Heat and Mass Transfer (2022). https://doi.org/10.11159/csp22.103

